PROCEEDINGS, 49th Workshop on Geothermal Reservoir Engineering
Stanford University, Stanford, California, February 12-14, 2024
SGP-TR-227

Investigation of Seismic Anisotropy in the Rotondo Granite by Crosshole Seismic Surveys

Kathrin Behnen, Marian Hertrich, Hansruedi Maurer and Domenico Giardini

Institute of Geophysics, ETH Zurich, Sonneggstrasse 5, CH – 8092 Zurich

Kathrin.behnen@erdw.ethz.ch

Keywords: Seismic Anisotropy, Active Seismic Measurements, Rock Characterization

ABSTRACT

In the framework of a geothermal project in the deep underground BedrettoLab, we have tested the hypothesis of stress-induced anisotropy by analyzing seismic wave propagation and considering the ambient state-of-stress. We present the results of comprehensive crosshole seismic surveys in three adjacent boreholes drilled into the undisturbed granitic host rock (Rotondo Granite) and we discuss novel approaches of data acquisition and analysis to fully exploit the information content offered by the recorded wavefields. In particular, we analyzed signals from various seismic sources recorded on different receiver types. Initial results of the measured traveltimes of both P- and S-waves indicate that the host rock can be described to a first order by a tilted transverse isotropic (TTI) model with a peak anisotropy of about 9%. However, there is also evidence that a more complex anisotropy model may be required to fully explain the seismic data, which could be indicative for a combination of structural and stress-induced anisotropy. This conjecture is currently being tested with more controlled laboratory-scale (cm to dm) experiments, as well as with a seismic inversion of crosshole data in a larger, more complex rock volume. Once the relation between seismic anisotropy, fracture orientations and the ambient stress field are better understood, this can potentially help to monitor changes in the stress field during geothermal operations for a better hazard assessment.

1. INTRODUCTION

It is well known that it is important to include seismic anisotropy, in the following simply referred to as "anisotropy", in seismic studies. Anisotropy does not only change the traveltimes from seismic waves, but also the path the wave is travelling, so that seismic tomography may be flawed, if anisotropy is neglected (Daley and Hron, 1977; Eken et al., 2012; Wong, 2010). This may affect, among others, the general rock characterizations and event localizations.

Reliable knowledge on the wave propagation, especially in an anisotropic rock can potentially be used to derive predominant directions of fracture networks or stress fields, as these parameters are known to cause anisotropy (Guo, 2019; Nur, 1971). However, also other parameters such as fault zones, bedding, foliation or mineral alignment can cause and control anisotropy in a rock (Barton, 2007; Al-Harthi, 1998; Song et al., 2004).

Since anisotropy can be caused by several features of a rock mass, the analysis of seismic data may be complex, and the question arises, if the individual causes can be identified. While some of the causative effects may be easy to exclude as a potential source, the influence of others might be less obvious. Especially in undisturbed, igneous rocks it can be challenging to identify the controlling mechanism, since they are often not directly visible, as it is the case for a layered sedimentary rock.

In our study, we analyzed the anisotropy in an undisturbed, homogeneous granitic rock. We employed the data of different seismic crosshole surveys, which were performed in the Bedretto Underground Laboratory for Geoenergies und Geosciences (BedrettoLab). The measured data were modeled with a tilted transverse isotropic (TTI) medium to describe the observed velocity field. The resulting model was then compared to other studies in the same rock volume to evaluate potential sources for the measured anisotropy.

2. THEORETICAL BACKGROUND

A hexagonal symmetry is commonly assumed for anisotropic media, also referred as a tilted transverse isotropic medium (TTI). Such a medium has a rotational symmetric velocity distribution around a symmetry axis with directional independent velocities in planes perpendicular to this axis. The associated elastic tensor is fully described by five independent parameters (Daley and Hron, 1977). In total seven parameters, the five elastic tensor elements and the direction of the symmetry axis described by dip and azimuth, are then required to fully describe the medium.

It is known that most rocks, especially metamorphic and sedimentary rocks, can be described by first order as a TTI medium (Thomsen, 1986; Alkhalifah, 2000; Carcione, 1987). There is no evidence that the symmetry in igneous rocks is more complicated, so we also assume a TTI medium in our case to model the measured velocities as a first approximation.

The mathematical fundamentals for a TTI anisotropy are given in Daley and Hron (1977), where the formulas for the normal velocity of all three wave types (quasi-compressional, quasi-shear and shear waves) are derived. In Thomsen (1986) these formulas are further simplified by using the Thomsen parameters instead of the parameters of the elastic tensor.

The Thomsen parameters (α, β, ε, δ, γ) are more intuitive and have a direct physical meaning. Thomsen (1986) describes the parameters as:

- α: P-wave velocity along the symmetry axis
- β: S1-wave velocity along the symmetry axis
- **ε**: fractional difference between vertical and horizontal P-Wave velocity
- **δ**: controlling parameter for near-vertical rays
- **γ**: fractional difference between vertical and horizontal S-Wave velocity

We make use of this mathematical description to fit a TTI model to our measured data to describe the rock volume of interest. In Thomsen (1986), the different S-waves are referred to as "horizontal" and "vertical", describing the polarization direction of the waves with respect to the elastic tensor. In our case, neither the orientation of the elastic tensor nor the polarization direction of the waves is known so we prefer calling the waves S1- and S2-waves. For the optimization, we decided to describe the velocity of the faster S1-wave with the formula of the SH-wave, as the wave polarized within the symmetry plane is usually the faster wave and the slower S2-wave with the formula of the SV-wave, which is assumed to be the slower one.

3. SITE DESCRIPTION

The data used in this analysis were collected in three adjacent boreholes, SB2.1, SB2.2 and SB2.3 of the BedrettoLab in Ticino, Switzerland. The laboratory is located in a 5.2 km long auxiliary tunnel, connecting the Bedretto Valley with the Furka railway tunnel. The lab is maintained and operated by ETH Zurich, to study techniques and ongoing processes during the production and operation of Enhanced Geothermal Systems (EGS). The laboratory provides the unique opportunity of a high spatial and temporal measurement distribution under realistic conditions of an EGS. The laboratory is located in the middle of the tunnel in the Rotondo granite, around 2 km away from the southern entrance. The overburden above the lab is about 1 km, so that the conditions in the laboratory are close to the real conditions of a geothermal field.

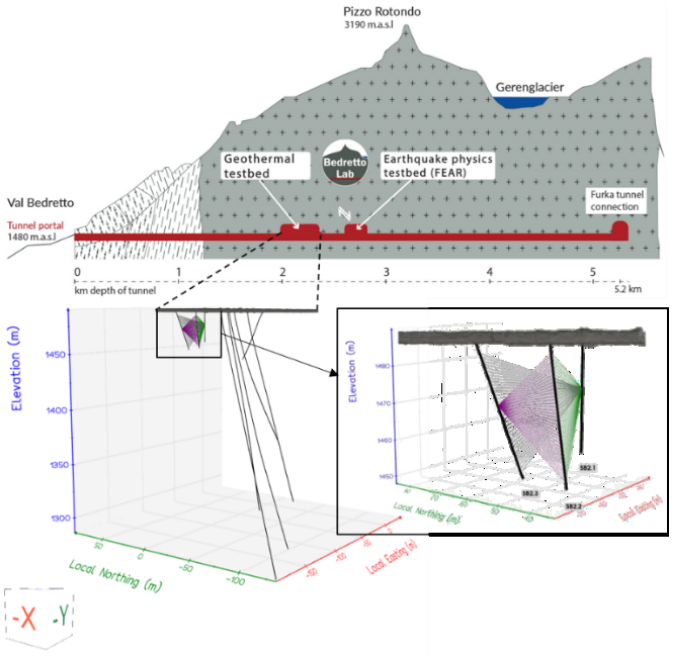

Figure 1: Top: Cross section along the Bedretto tunnel from the entrance in the Bedretto Valley (left end) to the Furka railway tunnel (right end). The boreholes used in this survey are located at the end of the main niche of the "geothermal testbed". Lower Left: Overview of the boreholes in the geothermal testbed. Lower Right: Detail view on the tripod boreholes. For each plane, exemplary rays are shown for one shot position in the middle of the adjacent boreholes.

Fig. 1 shows a cross section with the location of the tunnel in the mountain. The boreholes used for this study are placed at the end of the first niche, the geothermal testbed. Fig. 1 (lower row) sketches the boreholes penetrating the test volume as well as the shorter SB boreholes. While the longer boreholes in the test volume are mostly blocked by permanently installed sensors, the shorter SB boreholes are freely accessible for further studies. We used these shorter boreholes for several crosshole surveys as the boreholes penetrate the undisturbed granite and allow measurements in many different ray directions, which is crucial to get information about seismic anisotropy.

The boreholes have a length of 30 m (SB2.1) and 40 m (SB2.2, SB2.3), respectively. SB2.1 is pointing vertically downwards under the tunnel, while SB2.2 and SB2.3 have an azimuth of 225° and 135°, respectively and a dip of about 60-70°. As these three boreholes point in three different directions the boreholes are also referred to as "tripod boreholes". The configuration is also shown in Fig. 1, including exemplary ray directions covered in the surveys. The boreholes were originally drilled for detailed stress measurements. Therefore, detailed information on the local stress field is available for comparison.

4. DATA ACQUISITION AND ANALYSIS

Thomsen (1986) states that it is not sufficient to measure seismic velocities in two directions along and perpendicular to the symmetry axis. He shows that the near-horizontal velocity (horizontal means in the symmetry plane) is dominated by ε while the near-vertical velocity (subparallel to the symmetry axis) is dominated by δ.

In sedimentary and metamorphic rocks, the orientation of the elastic tensor is often known from the orientation of the bedding or foliation. In igneous rocks, the orientation is usually not known, so that seismic recordings in as many orientations as possible are required to fully describe the elastic tensor.

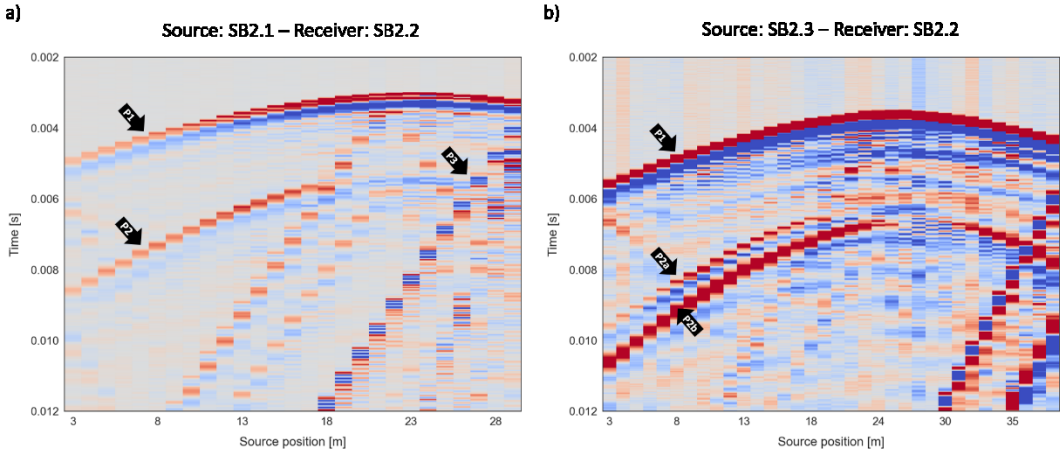

Figure 2: Exemplary receiver gather for the two planes. (a) Receiver gather for source positions in SB2.1 with 1m spacing, recorded on a hydrophone in SB2.2 at 26m depth. In this plane, the arrival of the P- and S1-wave is clearly detectable for most shot positions. (b) Receiver gather for source positions in SB2.3 with 1m spacing, recorded in SB2.2 at 23m depth. In this plane, the arrival of all three planes (P-, S1- and S2) can be detected for most shot positions.

In a first step, we performed a classical crosshole seismic survey. We used an undirected (P-wave) sparker as source in one of the boreholes, recording the data on hydrophones in the adjacent boreholes. With this configuration we covered all three planes with a spacing of 1 m for both, sources and receivers. Fig. 2 shows two exemplary receivers gather of this survey for different source positions.

In Fig. 2a, the receiver gather of measurements in the plane between borehole SB2.1 and SB2.2 (mainly E-W oriented) is shown. The arrival of the P-wave is clearly visible for all shot positions and can be picked accurately (P1). In the later parts of the signals, also the arrival of one S-wave is clearly distinguishable from the background noise, at least for shot positions in the upper part of the borehole (3 – 17 m) (P2). In this part, the S-wave arrival is separated enough from the P-wave arrival, so that it is not covered in the coda of the P-wave, as it is the case for deeper shot positions. For deeper shot positions, also different reflection and tube waves disturb the signal, covering the S-wave as well (P3). Fig. 2b shows the receiver gather of measurements in the plane between SB2.3 and SB2.2 (mainly N-S oriented). In this plane, the P-wave is also clearly visible for all source positions (P1) and the S-wave arrival is visible in the later parts of the signals. However, in this gather the arrival of two different S-waves with a small-time difference of 0.5 – 0.7 ms can be detected (P2a & P2b).

Splitting of S-waves is a phenomenon which can only occur in anisotropic media, so this feature clearly indicates seismic anisotropy in the tested rock volume. The splitting of the differently polarized waves depends on the wave velocities. These velocities differ only in some directions, depending on the orientation of the elastic tensor. This explains, why the splitting can only be observed in plane SB2.2 – SB2.3, but not in plane SB2.1 – SB2.2.

The source used in this survey is an undirected source. It produces a water bubble pressing against the borehole wall, thereby creating a longitudinal wave propagating through the rock. However, the water bubble is also expected to deform the borehole itself. This deformation can produce a transversal shear wave, which is recorded by the hydrophones.

In principle, transversal waves could be produced directly with a shear wave sparker, which radiates a pressure pulse in a preferred direction (www.Geotomographie.de/equipment/borehole-sources). We performed such measurements, but the resulting signal quality was poor and could not be used for further analyses.

We performed a further survey with the P-wave sparker, but we recorded the signals with 3C geophones, to get more insights in anisotropy. The separation of the wave field in three perpendicular components can give important information on the different wave forms, as differently polarized waves should appear on different components of the geophones. Unfortunately, we were not able to measure the orientation of the sensor in the borehole so that no absolute orientation of the three components but only the relative difference between the different components is known. Therefore, the data recorded with the 3C geophones were only used to compare the arrival times of the individual wave types.

The measured data of both, the hydrophone as well as the 3C geophone data are shown in Fig. 3. The upper row shows the results of the hydrophone data, the lower row those of the 3C geophones. Each stereonet plot shows the apparent velocities (source-receiver distance vs. measured travel time) for one of the three different wave types. The dot position represents the measurement direction (referred to as ray direction in the following, even though it is strictly speaking not the ray but a straight ray assumption). The dots are colorized by the apparent velocity along this ray.

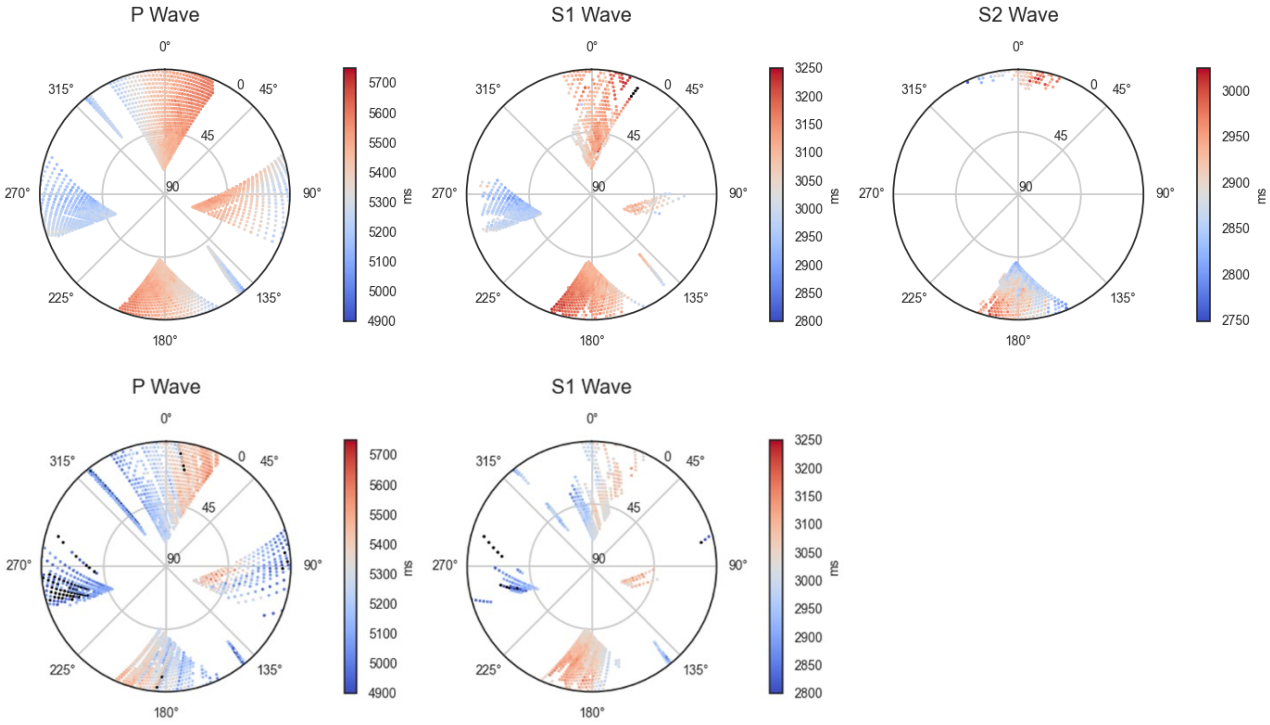

Figure 3: The apparent velocities for all picked arrival times on the hydrophones (upper row) and 3C geophones (lower row). Each stereonet represents the velocities for one wave tape. Each dot represents one source-receiver direction. On the 3C geophones, the slower S-wave cannot be picked accurate enough, so that only the faster S-wave is picked.

This representation does not only show the angular coverage we are able to measure with our set up but also velocity trends with the ray direction. The measurements between SB2.1 and SB2.3 span a straight, vertical plane, plotting in the stereonet as line with NW-SE direction. Measurements between SB2.1 and SB2.2 correspond to the triangles left and right with ray directions in E-W direction, hence rays from SB2.2 to SB2.3 plot in the upper and lower triangles with N-S direction.

The data sets of the hydrophones and 3C geophones are in good accordance to each other, showing a similar velocity pattern, but the uncertainties of the 3C data are higher, explaining the outliers (black) in these stereonets, so that we used this data set only to confirm the overall correctness of the hydrophone data.

The arrival of P- and S1-wave was clearly visible on both data sets for most source-receiver combinations. On the right stereonet only those ray directions are shown, where a separation of the S-waves is large enough to pick a second wave. We were not able to separate the waves clear enough on the 3C geophone data, so that we have S2-wave picks only from the hydrophone data set.

Both velocities, of the P- and S1-wave show a clear trend of faster velocities in NNE-SSW direction and lower velocities perpendicular to it in both data sets. This velocity trend, with a plane of faster velocities and slower velocities perpendicular to it, is the expected pattern for a TTI medium. While the S2-wave does not show such a clear trend, the appearance of a clearly separated S2-wave still fits the expectation. We were only able to pick a slower velocity in N-S direction but not perpendicular to it in E-W direction.

5. RESULTS

In this study we do not only aim to measure anisotropy but also to obtain a model that can explain these measurements sufficiently. We use the assumption of a TTI model, as the measured data already show the trend of a fast velocity plane and a symmetry axis of slower velocity. Furthermore, we assume that the illuminated rock volume is homogeneous as we have no indicator in the logging data or drill cores for any heterogeneities in terms of minerals or fault zones. We also assume straight rays between the sources and receivers, which is appropriate in our settings as no large anisotropy or velocity anomalies are expected in the test volume.

Based on these simplifications, we determined a first model guess by a grid search over the whole grid space. We minimized the offset between the modeled and measured P-wave velocities by differing the angles φ_0 and θ_0 of the symmetry axis and the Thomsen parameter ε and δ. This model is then used as initial model for an optimization algorithm, minimizing the misfit of all three wave types. The combination of the information of all three wave types further constrains the final velocity model, as the different wave types provide supplementary information on the elastic tensor and elastic tensor orientation.

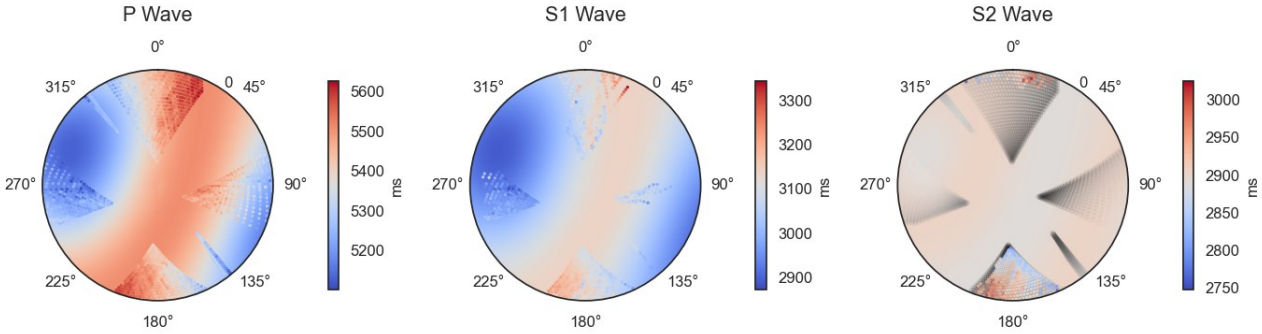

Figure 4: The stereonets show the optimized velocity model (background) and measured apparent velocities (foreground) for all three wave types. In the right stereonet plot, also the expected difference between the S1- and S2-waves are shown in grey, with dark colors representing high differences and light colors representing low differences.

The final model is shown in Fig. 4. The colored dots in the foreground are the measured data of the hydrophones, already shown in Fig. 3. The background color shows the velocity distribution calculated based on the optimized parameters φ_0, θ_0, γ, δ, ε, α and β. The stereonet of the S2-waves shows additionally the difference between the traveltime of S1- and S2-waves in grey, with high differences in dark colors and low differences in light colors. Measurement points which are hardly visible in the plot show directly a high accordance of the model with the measured data, as the same color bar for the measured data and the optimized model is used.

The optimized model explains the measured data of the P-waves quite well. The orientation of the symmetry plane and axis fits very well to the observed velocity pattern, only the magnitudes of the maximum and minimum velocities are not fully explained by the model. Smaller deviations can also be observed for rays in SW directions, in plane SB2.2-SB2.3. A similar fit is observed for the S1-waves, as the velocity distribution of the P- and S1-waves are equal in a TTI model and only the magnitudes of the velocities differ.

With our assumptions and data, we are not able to obtain a model which explains the S2-waves sufficiently. The velocity pattern shown in the S2-data, does not fit the expected pattern for a TTI model. The optimization algorithm tries to balance this contradicting pattern, resulting in a S2-wave velocity model with very little variations. However, the plot in Fig. 4 further shows that the different S-waves can only be clearly separated in directions, where the difference between the two wave types is assumed to be maximized.

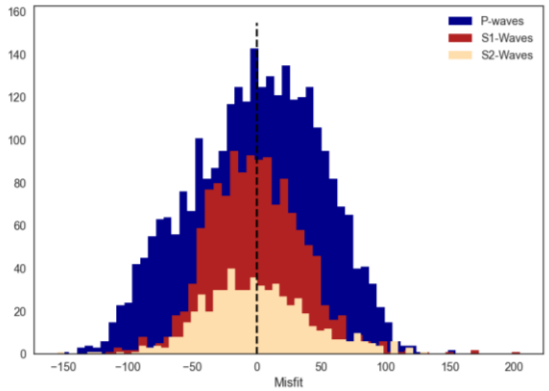

Figure 5: The misfit after the optimization for the three different wave types. The misfit is not fully Gaussian distributed but shows a slight shift towards positive values. Outliers are also only detected for positive values for all three wave types.

Fig. 5 shows the misfit distribution between the optimized models and the measured apparent velocities, separated for all three wave types. The misfit of all wave types shows a slightly shifted misfit distribution towards positive values, with more outliers with a positive misfit value. This indicates that the model tends to underestimate the measured velocities, which is mainly the case for rays in NNE-SSW direction. Such a pattern with an inhomogeneous misfit distribution indicates errors in the assumptions used to calculate the model, rather than only measurement errors.

6. DISCUSSION

For the interpretation of the results, the seismic anisotropy model determined in this study must be interpreted in the bigger context of the geological and geomechanical situation of the Rotondo granite. The measurements in the field allow us to interpret the absolute orientation of the elastic tensor in the field and not just the relative orientation of the tensor in a single rock sample, as it is the case for laboratory measurements. This knowledge of the in-situ orientation is highly important to identify potential sources, causing the anisotropy in the rock.

The different sources that are known to cause seismic anisotropy can be summarized in five groups: layering, fault zones, fabrics, fractures and stress-induced anisotropy (Barton, 2007). In the case of the undisturbed Rotondo granite, layering and fault zones can be excluded as potential sources. The logging data of the used boreholes as well as mapping on the tunnel wall close to the borehole mouths do not show any fault zones in the rock volume penetrated by the boreholes. Different studies on the geology of the rock also showed that the minerals in the rock samples of the boreholes do not show any alignment or preferred orientation (David et al., 2020; Ma et al., 2022; Jordan, 2019).

A likely option is that the measured anisotropy in our test bed is caused by a combination of the preferred orientation of fractures and the local stress field. The boreholes, used in this study, were originally drilled for extensive stress measurements, so that detailed results on the stress field and fracture network are available for comparisons with our data set.

The maximum principal stress around the tripod is found to be nearly vertical, the maximum horizontal stress is pointing towards N75°E to N87°E (Bröker, 2023). Microcracks perpendicular to the maximum stress direction are assumed to be closed and the material is assumed to be stiffer parallel to the horizontal stress, so that faster wave velocities are expected along the maximum stress directions (Nur and Simmons, 1969; Barton, 2007; Maitra, 2021).

The fracture network has a similar effect on the wave propagation. Waves travelling parallel to open fractures are assumed to be faster than waves perpendicular to it, crossing the fractures (Barton, 2007). The fractures around the tripod are vertical or subvertical and mainly N-S to NW-SE striking (Bröker et al., 2023; Jordan, 2019), suggesting faster velocities in this direction.

The orientations of the stress field, the fracture network and the anisotropy are summarized in Fig. 6. Black and grey lines represent the natural fractures mapped along the tunnel wall and in the boreholes, respectively. The arrows on the side point towards the maximum horizontal stress and the red line displays the symmetry plane of the TTI medium.

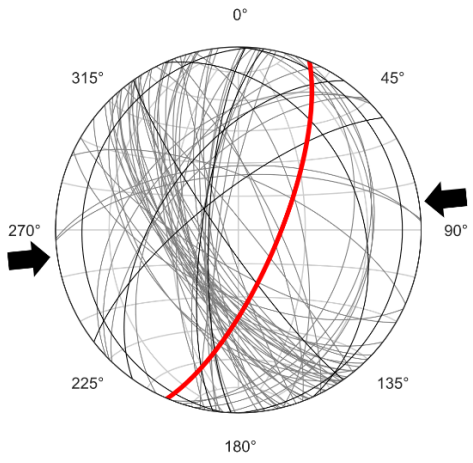

Figure 6: Representation of the natural fractures, stress field and seismic anisotropy. Fractures mapped in the tunnel are represented in black, fractures mapped in the tripod are represented in grey. The arrows on the side point towards the maximum horizontal stress. The red line shows the symmetry plane of the TTI medium.

The symmetry axis, representing the direction of faster P- and S1-wave velocities, does not coincide with the natural fracture orientation or the maximum horizontal stress but is in right in between. Therefore, a combination of the fracture orientation and the adjacent stress field is a possible source for the anisotropy.

7. CONCLUSION

A tripod of boreholes located in the BedrettoLab was used for an extensive study of the seismic anisotropy in the Rotondo Granite. The orientation of the boreholes is favorable for crosshole seismic surveys as many different ray orientations can be covered. Using a P-wave

sparker as the source and hydrophones as the receiver provides a meaningful data set. 3C geophone data can be used as a supplement, especially to verify the arrival times of the P-waves.

The measured apparent velocities can be modelled by a TTI model. The faster P- and S1-waves lie within the symmetry plane, while the slowest directions are detected perpendicular to it. The uncertainties in the model can be explained by the different simplifications we used: a homogeneous model, straight rays and a hexagonal symmetry.

The measurement of the seismic anisotropy in the field allows the comparison of the result with different other studies carried out in the same test bed. We compared our velocity model with the geology and geomechanical properties of the Rotondo Granite around the tripod boreholes. We conclude that a combination of the natural fractures and the in-situ stress field can explain the anisotropy best. Other parameters such as fault zones, mineral alignments or layering of the rock can be excluded as potential sources but we cannot distinguish the influence of the fracture network and stress field any further.

Separating the different S-wave types more precisely could help to constrain the model further. Also, a more complicated model could be helpful to understand the wave propagation more in detail.

REFERENCES

Al-Harthi, A. A. (1998). Effect of planar structures on the anisotropy of Ranyah sandstone, Saudi Arabia. Engineering Geology, 50(1–2), 49–57. https://doi.org/10.1016/S0013-7952(97)00081-1

Alkhalifah, T. (2000). An acoustic wave equation for anisotropic media. Geophysics, 65(4), 1239–1250. https://doi.org/10.1190/1.1444815

Barton, N. (2007). Rock Quality, Seismic Velocity, Attenuation and Anisotropy.

Bröker, K., Ma, X., Zhang, S., Doonechaly, N. G., Hertrich, M., Klee, G., Green-Wood, A., Caspari, E., Giardini, D., & Greenwood, A. (2023). Constraining the stress field and its variability at the BedrettoLab: Elaborated hydraulic fracture trace analysis. https://dx.doi.org/10.2139/ssrn.4706040

Carcione J. M., & Kosloff D. (1987). Wave-Propagation Simulation in an Elastic Anisotropic (Transversely Isotropic) Solid. https://academic.oup.com/qjmam/article/41/3/319/1851937

Daley, P. F., & Hron, F. (1977). Reflection and transmission coefficients transversely isotropic media. In Bulletin of the Seismological Society of America (Vol. 67, Issue 3). http://pubs.geoscienceworld.org/ssa/bssa/article-pdf/67/3/661/5320942/bssa0670030661.pdf

David, C., Nejati, M., & Geremia, D. (2020). On petrophysical and geomechanical properties of Bedretto Granite. ETH Zurich.

Eken, T., Plomerová, J., Vecsey, L., Babuška, V., Roberts, R., Shomali, H., & Bodvarsson, R. (2012). Effects of seismic anisotropy on P-velocity tomography of the Baltic Shield. Geophys. J. Int, 188, 600–612. https://doi.org/10.1111/j.1365-246X.2011.05280.x

Guo, T., Wang, H., Guo, Y., Zhang, J., Jiang, M., Chen, P., & Kong, X. (2019). Fracture Prediction based on an Improved Anisotropy Inversion: a Shale Reservoir Fracture Prediction Case Study. SEG Technical Program Expanded Abstracts, 414–418. https://doi.org/10.1190/segam2019-3215462.1

Jordan, D. (2019). Geological Characterization of the Bedretto Underground Laboratory for Geoenergies. https://doi.org/10.3929/ethz-b-000379305

Ma, X., Hertrich, M., Amann, F., Bröker, K., Gholizadeh Doonechaly, N., Gischig, V., Hochreutener, R., Kästli, P., Krietsch, H., Marti, M., Nägeli, B., Nejati, M., Obermann, A., Plenkers, K., Rinaldi, A. P., Shakas, A., Villiger, L., Wenning, Q., Zappone, A., … Giardini, D. (2022). Multi-disciplinary characterizations of the BedrettoLab – a new underground geoscience research facility. Solid Earth, 13(2), 301–322. https://doi.org/10.5194/se-13-301-2022

Maitra, M., & Al-Attar, D. (2021). On the stress dependence of the elastic tensor. Geophysical Journal International, 225(1), 378–415. https://doi.org/10.1093/gji/ggaa591

Nur A. (1971). Effects of stress on velocity anisotropy in rocks with cracks. J Geophys Res, 76(8), 2022–2034. https://doi.org/10.1029/jb076i008p02022

Nur A, & Simmons G. (1969). Stress-induced velocity anisotropy in Rock: An Experimental Study. J Geophys Res, 74(27), 6667–6674. https://doi.org/10.1029/jb074i027p06667

Song, I., Suh, M., Woo, Y. K., & Hao, T. (2004). Determination of the elastic modulus set of foliated rocks from ultrasonic velocity measurements. Engineering Geology, 72(3–4), 293–308. https://doi.org/10.1016/J.ENGGEO.2003.10.003

Thomsen, L. (1986). Weak elastic anisotropy. Geophysics, 51(10), 1954–1966. https://doi.org/10.1190/1.1442051

Wong, J. (2010). Fermat's principle and ray tracing in anisotropic layered media. In Ray tracing in anisotropic layers CREWES Research Report (Vol. 22).